EPJ Web of Conferences **63**, 03002 (2013)
DOI: 10.1051/epjconf/ 20136303002

Stellar neutron capture rates – key data for the *s* process

F. Käppeler[1,a]

[1] *Karlsruhe Institute of Technology, Campus North, IKP,76021 Karlsruhe, Germany*

Abstract. Neutron reactions are responsible for the formation of the elements heavier than iron. The corresponding scenarios relate to the He- and C- burning phases of stellar evolution (*s* process) and to supernova explosions (*r* and *p* processes). The *s* process, which is characterized by low neutron densities, operates in or near the valley of β stability and has produced about half of the elemental abundances between Fe and Bi in the solar system and in the Universe. Because the *s* abundances are essentially determined by the (n,γ) cross sections along the reaction path, accurate neutron data constitute the key input for *s* process studies. Important constraints for the physical conditions at the stellar sites can be inferred by comparison of the abundance patterns from current *s*-process models with solar system material or presolar grains. The experimental methods for the determination of stellar (n,γ) rates are outlined at the example of recent cross section measurements and remaining quests will be discussed with respect to existing laboratory neutron sources and new developments.

1 Introduction

The concept of neutron capture nucleosynthesis as the origin of the heavy elements beyond the Fe group has been formulated half a century ago in the pioneering work of Burbidge, Burbidge, Fowler and Hoyle (B^2FH) [1] and of Cameron [2]. Accordingly, the elements heavier than iron are predominantly produced either by the slow (*s*) or the rapid (*r*) neutron capture process, which are characterized by their typical neutron capture times with respect to the average β-decay half lives. Both processes are contributing about half of the observed solar abundances between Fe and U. A third process, the so-called *p* (photodissociation) process, is responsible for the origin of about 30 rare, proton-rich nuclei, but does not contribute significantly to the synthesis of the elements in general (<1%).

Since the formulation of these concepts, considerable progress has been achieved in the quantitative description of the *s* process, which meanwhile provides rather detailed information of the *s* component in the solar system abundances as well as of the role the *s* process plays in galactic chemical evolution. Two *s* components have been identified, the main and the weak *s* process, which are connected with the specific burning phases in stars of different mass. Initially, a third component, the strong *s* process, had been invoked for explaining part of the observed ^{208}Pb abundance, but was eventually ascribed to the main *s* process in low-metallicity stars [3].

The main *s* process, by far the most studied process, occurs in the He-rich intershell of thermally pulsing asymptotic giant branch (AGB) stars with $M \leq 3M_\odot$ ($M_\odot$ denotes the mass of the sun) and produces predominantly nuclei between ^{90}Zr and ^{209}Bi. At this stage, energy generation occurs by alternate episodes of radiative H burning and convective He burning in a comparably thin shell around the inert C/O core. Along with H burning, neutrons are liberated by the $^{13}C(\alpha,n)^{16}O$ reaction at temperatures of $T_8 \approx 1$ (T_8 means T in units of 10^8K), yielding neutron densities of about 10^7 cm^{-3}. Because there are only few seed nuclei in this thin shell, the neutron/seed ratio is high and the *s* process operates very efficiently over a long period of time. During the subsequent convective He flashes, the freshly synthesized material is mixed and diluted with the He intershell and is again exposed to neutrons liberated by the $^{22}Ne(\alpha,n)^{25}Mg$ reaction at temperatures $T_8 \approx 2.5$. The second neutron exposure is rather weak and not sufficient to produce *s* isotopes on a grand scale but strong enough to determine the isotope ratios of *s*-process branchings. After the He flash, where peak neutron densities of 10^{10} cm^{-3} are reached, part of the freshly synthesized material is mixed with the envelope and brought to the surface of the star, where it is detectable by optical spectroscopy. A famous example is the early discovery of Tc lines by Merrill [4], which confirmed that heavy elements are produced during the red giant phase of stellar evolution.

The weak *s* component, which is responsible for the production of nuclei between iron and yttrium ($56 < A < 90$), takes place during convective core-He burning in massive stars ($M \geq 8M_\odot$), where temperatures reach (2.2 - 3.5)$\times 10^8$ K, thus marginally activating the $^{22}Ne(\alpha,n)^{25}Mg$ neutron source. Because the resulting neutron exposure is rather limited, the *s*-process reaction flow cannot overcome the bottleneck caused by the small cross sections of the isotopes with closed neutron shells at N = 50. However, most of the material in the core is reprocessed by the following burning stages and only a part survives

[a] e-mail: franz.kaeppeler@kit.edu

in the outer layers and is ejected during the final supernova explosion. A second neutron exposure occurs during convective carbon shell burning in massive stars [5, 6], where neutrons are produced mostly by the remaining ^{22}Ne$(\alpha,n)^{25}$Mg, but also via ^{17}O$(\alpha,n)^{20}$Ne and ^{13}C$(\alpha,n)^{16}$O. The high temperatures during carbon burning of $T_9 \approx 1$ cause high neutron densities, which start at about $10^{11} - 10^{12}$ cm^{-3} and then decrease exponentially.

The nucleosynthesis yields of the weak component in massive stars are also important for the *r* process, since they determine the composition of a star before the supernova explosion. In contrast to the *s* process, where neutron capture times of the order of days to years confine the reaction path to or close to the valley of β stability, extremely high neutron densities of $\geq 10^{22}$ cm^{-3} are reached in the *r* process, giving rise to capture times of the order of milliseconds. These parameters are clearly indicating an explosive scenario for the *r* process either related to supernovae or neutron star mergers. In either case, the extreme neutron densities imply that (n,γ) reactions are becoming much more rapid than β decays, thus driving the reaction path to the region of very neutron-rich nuclei at the limits of stability. The initial reaction products of the explosive *r* process, which lasts for about a second, are highly β-unstable and decay after the explosion back to the valley of stability, where they mix with the *s* abundances.

The reaction paths of the *s* and *r* process are sketched in Fig. 1. The neutron-rich isotopes outside the *s* path can be ascribed to the *r* process. Apart from these *r*-only isotopes the *r* process contributes also to most of the other isotopes, provided that they are not shielded by stable isobars. The corresponding ensemble of the *r*-shielded, *s*-only isotopes is important for the separation of the respective abundance distributions and, more importantly, to set constraints for the overall *s*-process efficiency and for the parameters governing the abundance pattern in *s*-process branchings. The subset of *r*-only nuclei can be used for calibration of the abundance contributions from the *r* process. About 32 stable isotopes on the proton-rich side, which cannot be produced by stellar neutron reactions, are attributed to the *p* process, which is likely to occur also in supernova explosions [7]. With very few exceptions, these *p* abundances are much smaller than the *s* and *r* components.

2 Stellar neutron capture cross sections

Presently, experimental techniques for (n,γ) measurements have reached a stage, where the 1-2% accuracy level required for sufficiently detailed analyses of the *s*-process abundance patterns can be met [8, 9]. While this level has been achieved so far only for a minority of the relevant isotopes, a large number of cross sections with uncertainties in excess of 10% await improvement, still including many remaining key nuclei. With a few exceptions, experimental data for the important unstable branch point isotopes are still completely missing.

In contrast to the favorable situation of the *s* process, where mostly stable isotopes are involved, explosive nucleosynthesis scenarios of the *r* and *p* processes imply complex reaction paths far from stability, which must be described by huge networks including several thousand reactions. By far most of these reaction rates have to be obtained by statistical model calculations [10, 11]. Nevertheless, experimental data for stable and as many unstable isotopes as possible are required for testing the necessary extrapolation to the region of unstable nuclei.

To cover the range of *s*-process temperatures between $T_8 = 1$ to 9, experimental neutron capture cross sections are needed over an energy range from about 300 eV to several hundred keV, which then have to be folded with the fully thermalized neutron energy distribution in the stellar plasma. These Maxwellian averaged cross sections (MACS) are defined as

$$\langle\sigma\rangle_{kT} = \frac{\langle\sigma v\rangle}{v_T} = \frac{2}{\sqrt{\pi}} \frac{\int_0^\infty \sigma(E_n)\, E_n\, \mathrm{e}^{-E_n/kT}\, dE_n}{\int_0^\infty E_n\, \mathrm{e}^{-E_n/kT}\, dE_n}, \qquad (1)$$

where $E_n = E_n^{lab}(A/(A+1))$ denotes the total kinetic energy in the center-of-mass system, E_n^{lab} the laboratory neutron energy, $v_T = \sqrt{2kT/m}$ the mean thermal velocity, and m the reduced mass for the neutron-target system.

MACS values are required for all nuclei and all temperatures involved in a particular scenario, essentially from ^{12}C up to the Pb/Bi region. It is important to note that the high *s*-process temperatures imply that excited nuclear states are in thermal equilibrium by the intense and energetic thermal photon bath, resulting in a significant population of low-lying states. The effect of neutron captures in these excited states has to be determined by theory and may require significant corrections to the experimental data [12].

The thermal environment can have also a considerable impact on the weak decays of the unstable branch point isotopes along the reaction chain: The rate for β^--decays may be dramatically enhanced if the excited states have much shorter half-lives than the ground state. The rates for EC-decay are affected by the high degree of ionization in two ways: a reduction due to the loss of K-shell electrons is partly compensated by capture of free electrons. Bound beta decay, where electrons are emitted in unoccupied atomic orbits, can result in a dramatic enhancement as well. For a full discussion of *s*-process beta decays see Refs. [13, 14].

3 Experimental methods

3.1 Time-of-flight experiments

Time-of-flight (TOF) measurements are essential for obtaining energy-differential neutron capture cross sections over a sufficiently large energy range so that MACS values can be determined from these data for any stellar temperature of interest. Recent developments and improvements in pulsed neutron sources and detection techniques have led to (n,γ) cross section measurements with improved accuracy, in many cases with uncertainties of 2 - 4%.

As far as the laboratory neutron sources are concerned, spallation reactions induced by energetic particle beams

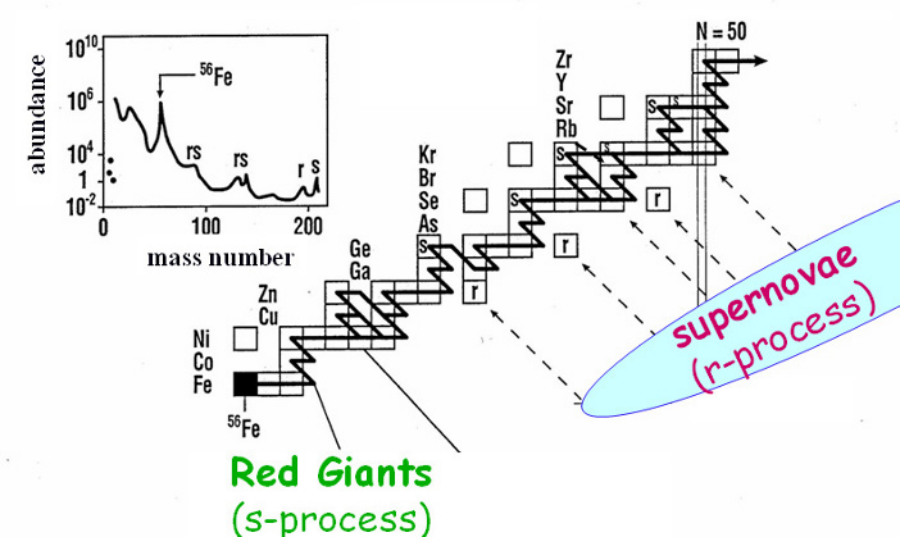

Figure 1. Illustration of the main neutron-capture processes responsible for the formation of the nuclei between iron and the actinides. The reaction path of the *s* process follows the stability valley because the neutron capture times are much slower than β decay on average. The abundance contributions from the *r* process (dashed arrows) are mixing with the *s* component, except where the *s*-only isotopes are shielded by stable isobars. Note also the occurrence of branchings in the *s*-process path at sufficiently long-lived unstable nuclei. The branching points give rise to a local abundance pattern that carries important information on neutron density and temperature at the *s*-process site. The small cross sections at magic neutron numbers introduce another important constraint for the *s* process because they act as bottle necks for the reaction flow.

constitute the most prolific pulsed sources of fast neutrons for TOF measurements. Presently, spallation sources in routine operation are LANSCE at Los Alamos [15], the n_TOF facility at CERN [16, 17], and ANNRI at J-PARC [18]. The main advantage of these facilities is the outstanding efficiency for neutron production due to the high primary proton beam energies, reaching 300 neutrons per incident proton at n_TOF, for example. Spallation sources are providing a wide neutron energy range and are operated at rather low repetition rates, typically between 0.4 and 50 Hz, while still maintaining high average intensities. Rather high intensities can also be achieved via (γ, n) reactions at electron linear accelerators, such as GELINA at Geel, Belgium, by bombarding heavy metal targets with electron beams of typically 50 MeV. All these facilities provide very good resolution in neutron energy and have been extensively used to study the resolved resonance region.

The spectrum of keV neutron facilities includes also small accelerators, where neutrons are produced by nuclear reactions, such as the ^{7}Li$(p,n)^{7}$Be reaction, which offer the possibility of tailoring the neutron spectrum exactly to the stellar energy range. Limitations in source strength can be compensated by low backgrounds and the use of comparably short neutron flight paths [19, 20].

Current TOF measurements of (n,γ) cross sections are based on two types of detectors. Total absorption calorimeters are designed to detect the full energy sum of the γ-ray cascade emitted in the decay of the compound nucleus, which corresponds essentially to the neutron separation energy of the captured neutron. Because this energy represents the best signature of a capture event, 4π detector arrays with an efficiency close to 100% are the most direct way to unambiguously identify (n,γ) reactions and to determine capture cross sections with good accuracy. Such calorimeters are designed either in spherical geometry, using BaF_2 crystals arranged in a fullerene-type configuration with each module covering the same solid angle with respect to the central sample [21–23], or in a barrel-type geometry, where the sample is surrounded by layers of hexagonal crystals [24, 25].

The main problem in using calorimeter type detectors arises from their response to neutrons scattered in the sample. Although the BaF_2 scintillator is selected to consist of nuclei with small (n,γ) cross sections, about 10% of the scattered neutrons are still captured in the scintillator. While the related background can be handled in most measurements, it may complicate the analysis of resonances with very small capture-to-scattering ratios.

The problem of neutron sensitivity is largely avoided by using comparably small, hydrogen-free liquid scintillators in combination with the pulse-height weighting technique (PHWT) [26], in particular since the second generation of detectors, which are based on deuterated benzene (C_6D_6), has been designed to minimize backgrounds due to scattered neutrons to a practically negligible level [27]. With advanced Monte Carlo codes, realistic descriptions of the detector response and of the weighting functions (WF) could be obtained on the basis of detailed computer models of the experimental setup [28–31]. Such refined simulations have been shown to reduce the systematic uncertainty of the PHWT to about 2% [30]. Although the

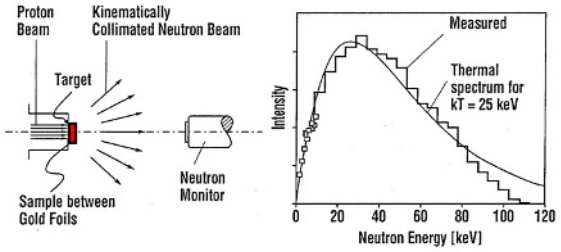

Figure 2. Left: Schematic sketch of the activation setup. Right: The quasi-stellar neutron spectrum obtained with the ^{7}Li$(n,\gamma)^{7}$Be reaction (histogram and symbols) compared to a true Maxwell-Boltzmann distribution for a thermal energy of kT = 25 keV [32].

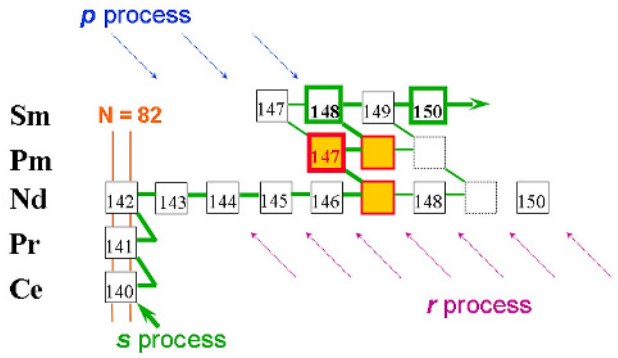

Figure 3. The s-process reaction flow in the mass region $140 \leq A \leq 150$ including the crucial s-only isotope ^{142}Nd and the branchings at A = 147, 148.

efficiency of C_6D_6 detectors is only about 20%, they are clearly of advantage in studies of resonance-dominated cross sections with very small capture-to-scattering ratios.

3.2 Activation with quasi-stellar neutrons

The activation method represents a well established and accurate approach for MACS measurements at a thermal energy of kT = 25 keV by irradiating samples in a quasi-stellar neutron spectrum that can be produced via the ^{7}Li$(p,n)^{7}$Be reaction [32, 33]. Such a spectrum is obtained by using a proton beam energy of E_p = 1912 keV, 30 keV above the reaction threshold. With this choice of E_p, neutrons are kinematically collimated into a forward cone of 120 deg opening angle. The effect of fluctuations in beam intensity during the irradiations can be corrected by continuously monitoring the neutron yield by means of a ^{6}Li-glass detector.

With typical beam intensities of 100 μA, neutron intensities of 3×10^{9} s^{-1} can be reached, orders of magnitude higher than in TOF experiments. Accordingly, the activation method offers unique sensitivity. Further advantages are (i) that isotopically enriched samples are not required, because the reaction products are identified by their characteristic γ radiation, and (ii) that contributions from the direct radiative capture (DRC) channel are automatically considered. A sketch of the experimental setup and the comparison of the resulting quasi-stellar neutron spectrum with a true Maxwell-Boltzmann distribution are shown in Fig. 2. Note that the experimental spectrum in the right panel of Fig. 2 falls below the Maxwell-Boltzmann distribution above 80 keV and is truncated at a neutron energy of 106 keV. Meanwhile, it has been found that the high-energy part of the spectrum can be better approximated by using an energy-broadened proton beam with a spread of about 20 keV [34, 35].

4 The role of key cross sections

The key isotopes ^{142}Nd and ^{147}Pm, which are included in the s-process reaction flow shown in Fig. 3, are used to illustrate the crucial role of stellar (n,γ) cross sections for testing the validity of stellar s-process models related to He shell burning in thermally pulsing AGB stars. In addition, the measurement of the small cross sections of abundant light isotopes and their role as neutron poisons are discussed at the example of ^{13}C.

4.1 ^{142}Nd: confirming the stellar model for the main s process

The s-only isotope ^{142}Nd belongs to the stable neutron-magic nuclei with N=82, which act as bottle necks for the reaction flow. The small MACS values of these isotopes prevent that flow equilibrium is locally achieved in the mass range $A = 138 - 142$. Because the s-abundance distribution below and above that critical region is well constrained by the important s-only isotopes ^{124}Te and ^{150}Sm, the N=82 region provides a crucial test for the mean neutron exposure of the main s-process component, τ_0 [36]. In particular, the resulting ^{142}Nd abundance is sensitively probing the way an s-process model is treating the reaction flow across the bottle-neck region.

The classical steady s-process model [36, 37] has long been considered a useful tool for describing the s-process abundances and for estimating the physical conditions during the s process via the abundance pattern of the various branchings. The left panels of Fig. 4 illustrate the abundances of the s-only isotopes between ^{130}Xe and ^{160}Dy as obtained with the classical model before and after an accurate cross section of ^{142}Nd became available. The new MACS of ^{142}Nd [38], which was 25% lower than the value used before, gave rise to a significant 12% excess of ^{142}Nd compared to the solar abundance. In view of the 2% uncertainty of the quoted value, this discrepancy revealed the first convincing inherent inconsistency of the classical model, indicating that the simplifying assumptions of this approach are not adequate for describing the true stellar scenario.

Although necessarily more complex, realistic prescriptions on the basis stellar s-process scenarios have been developed as sketched in Sec. 1. For the main component (including the mass region of Fig. 4) the He shell burning

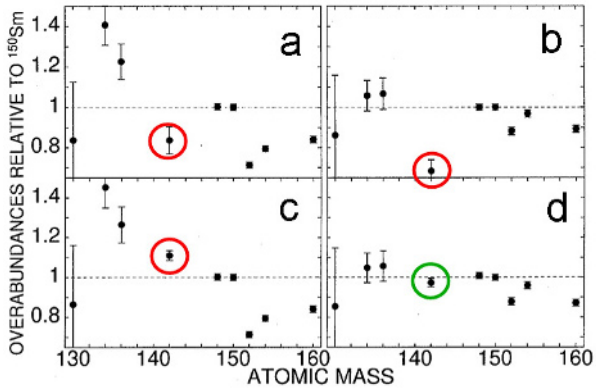

Figure 4. The overproduction factors of the *s*-only isotopes relative to solar material (normalized at ^{150}Sm) in the mass region $130 \leq A \leq 160$. While a perfect model would always yield factors of unity, the upper panels ("a" for the classical and "b" for the stellar model) indicate an underproduction of ^{142}Nd when the previous cross section was used for this key isotope, regardless of the *s*-process model. The lower panels illustrate the effect of the improved, accurate cross section of ^{142}Nd [38], which is clearly favoring the physical stellar model (d) over the purely phenomenological, classical approach (c).

episodes in low mass AGB stars have been shown to reproduce the *s* abundances to better than 10% [39]. Contrary to the classical picture, this rather complex model is characterized by two neutron sources operating with very different strength and at different neutron densities and temperatures.

The success of the stellar model compared to the classical approach is illustrated in the right panels of Fig. 4, showing that the new ^{142}Nd cross section [38] resulted in a perfect reproduction of the solar value (panel d). Moreover, there is clearly an improved overall agreement for the other *s*-only isotopes as well.

4.2 Branchings as diagnostic tools: ^{147}Pm

Branchings in the reaction path are the result of the competition between neutron capture and β-decay whenever an isotope with a half-life comparable to the neutron capture time is encountered. This competition is expressed by a branching factor $f_\beta = \frac{\lambda_\beta}{\lambda_\beta + \lambda_n}$ that depends formally on the β-decay rate $\lambda_\beta = \ln 2 / t_{1/2}$ and on the neutron capture rate $\lambda_n = n_n v_T \langle\sigma\rangle$ with n_n being the neutron density, v_T the mean thermal velocity, and $\langle\sigma\rangle$ the MACS for the radioactive branch point nucleus.

The *s*-process branchings are producing a local abundance pattern that includes an *s*-only nucleus, which is partially bypassed by the reaction flow. Accordingly, these nuclei exhibit a smaller $\langle\sigma\rangle N$ value than what is characteristic of the full reaction flow and thus provide a measure for the strength of the branching. The different ratios of neutron capture and β-decay in the various branchings along the *s*-process path from Fe to Bi represent viable and stringent tests of *s*-process prescriptions and, hence, for models of the He and C burning phases of stellar evolution.

So far, most branching analyses are based on solar isotope patterns [8, 39], but it should be noted that important information on the *s*-process neutron density can be derived directly from spectroscopic data of individual AGB stars via the branchings at ^{85}Kr and ^{93}Zr [40] or from analyses of presolar grains preserved in primitive meteorites [41].

The branching at ^{147}Pm (Fig. 3) is part of a series of important branchings in the lanthanide region. Apart from the "normal" branch point isotopes ^{147}Nd, ^{147,148}Pm, which are only sensitive to the stellar neutron density, the half-lives of ^{151}Sm, ^{152,154}Eu exhibit a temperature dependence [13], which makes these branchings potential thermometers for the *s*-process environment [42, 43].

The measurement of neutron capture cross sections on unstable isotopes is complicated by the radioactivity of the sample. For many of the branch point isotopes, this results in an immense γ background that can hardly be handled by the detectors and hampers the safe identification of capture events in the sample. Also, the required samples are most often not available in amounts needed for TOF experiments. Therefore, measurements have resorted to the activation technique. The excellent sensitivity of this method permitted the use of samples in the μg range, thus reducing the radiation hazards by several orders of magnitude.

The example of ^{147}Pm is quite illustrative in this respect, because the activation was performed with only 28 ng of material, the smallest sample used in (n,γ) studies at keV energies so far. To compensate for the low induced activities that can be obtained with such a small sample, an optimized setup for γ counting had to be used by placing the irradiated sample between two large Clover-type HPGe detectors in very close geometry. For suppression of the still dominant background from the decay of ^{147}Pm ($t_{1/2}$ = 2.62 yr), one had to go a step further, using the eight-fold geometry of the two Clover detectors for the coincident detection of the (915+550) keV γ cascade in the decay of ^{148}Pm. In this way, the dominant ^{40}K background could be sufficiently reduced to determine the stellar cross section of ^{147}Pm with an uncertainty of 14%, leading to a mean neutron density of $n_n = 4.9 \pm 0.6$ cm^{-3} [44].

4.3 ^{13}C: a potential neutron poison

Limits of MACS measurements with the activation method refer to cases where the induced activity is very low, uncertain, or difficult to detect. For such reactions, accelerator mass spectrometry (AMS) offers a powerful alternative with the important advantage compared to decay counting that it is independent of the half-lives and decay properties of the reaction products. The main feature of AMS is the unsurpassed sensitivity for specific nuclides, much higher than can be obtained with conventional mass spectrometry, disadvantages are often elaborate sample preparation and the destruction of the sample by the measurement.

AMS has first been applied to neutron capture reactions in *s*-process environments for ^{62}Ni by Nassar *et al.* [45] and subsequently to a number of target nuclei including ^{40}Ca, ^{58}Ni, ^{62}Ni, and ^{78}Se [46–48]. The ^{13}C$(n,\gamma)^{14}$C

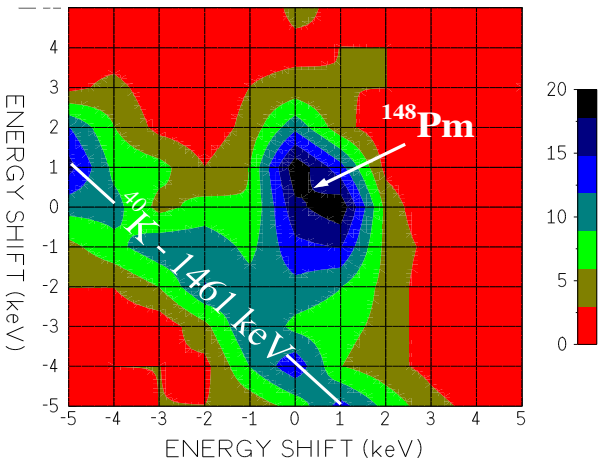

Figure 5. Discrimination of the induced ^{148}Pm activity against the 1461 keV background from ^{40}K by coincident detection the (915+550) keV γ cascade in the decay of ^{148}Pm (from Ref. [44]).

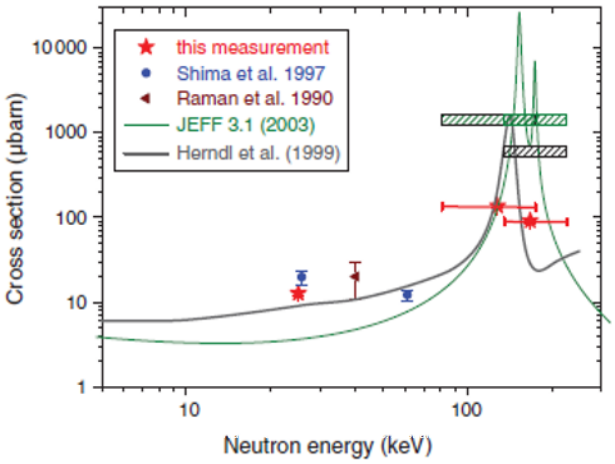

Figure 6. Experimental cross sections for the ^{13}C$(n,\gamma)^{14}$C reactions in the keV neutron energy region together with calculated values [50] and recent evaluations from the JEFF-3.1 data library. The width of the experimental neutron energy distributions are indicated by horizontal bars. The shaded areas correspond to spectrum-averaged cross sections derived from the calculated data of Ref. [50].

reaction was studied as part of a recently completed series of measurements [49] and represents a typical example for combining activation at keV neutron energies with subsequent AMS detection of the long-lived reaction product ^{14}C.

An interesting feature of this reaction is the strength of the resonance at E_n = 143 keV (Fig. 6), which interferes with the p-wave contribution of the direct capture component. At temperatures above T_8 = 3 the reaction rate is dominated by the 143 keV resonance, at lower temperatures by the p-wave and s-wave contributions. The calculations [50] are in reasonable agreement with two previous experiments [51, 52], but exhibit a significant discrepancy compared to the most recent evaluation of JEFF-3.1, which is consistently higher than the calculation, culminating in a 25 times higher peak value for the 143 keV resonance.

This discrepancy, which is important for the role of ^{13}C as an *s*-process neutron poison, was studied using the activation technique [53]. The samples were irradiated at the Karlsruhe Institute of Technology in the quasi-stellar neutron spectrum for the direct determination of the MACS at kT = 25 keV, and also using neutron spectra with 123 and 178 keV mean energy to investigate the effect of the 143 keV resonance. After the irradiations the produced amount of ^{14}C was quantitatively determined by AMS. In this experiment, the cross sections could be obtained with uncertainties of 7 to 12%.

Fig. 6 shows that the results of the AMS measurement at 25 keV are in fair agreement with the previous experimental [51, 52] and theoretical [50] data, but about two times higher than the JEFF-3.1 evaluation. For the two higher neutron energies a striking discrepancy was found with respect to the strength of the 143 keV resonance, which turned out to be a factor of 10 lower than the calculation of Herndl *et al.*[50] (indicated by the horizontal bars in Fig. 6). Accordingly, the poisoning effect of that resonance is much less significant than previously assumed.

5 Status and Outlook

The current MACS status is collected in the KADoNiS database [54], which contains an almost complete set of experimental MACS values for the 279 stable isotopes on the *s*-process path. KADoNiS also includes data for 77 radioactive nuclei, albeit this subset still has to rely on theoretical calculations with the HF statistical model (e.g. [10]). An important aspect of the MACS data refers to the accuracy needed for meaningful abundance predictions. On average, cross sections should be available with an accuracy of 5% or better, but uncertainties as low as 1-2% are mandatory for a number of key isotopes, e.g., for the 33 *s*-only nuclei on the *s*-process path. Examples for this species are ^{148,150}Pm in Fig. 3.

Similarly accurate data are needed for the interpretation of the *s*-process signatures of presolar grains [41] that concern about 70 isotopes. The discovery of presolar grains in primitive meteorites opened a new window to stellar nucleosynthesis and galactic chemical evolution, because they represent material from individual stars, which survived the high temperature phase during the formation of the solar system. Accordingly, analyses of such grains provide insight into the sensitivity of the *s* process to stellar mass and metallicity.

Although experimental data exist for most stable isotopes of interest for the *s* process, the criteria of completeness and accuracy are met only in a minority of cases. From the standpoint of accuracy, this aspect is illustrated in Fig. 7, where the respective uncertainties are plotted versus mass number. Though the requested uncertainties have been locally achieved, further improvements

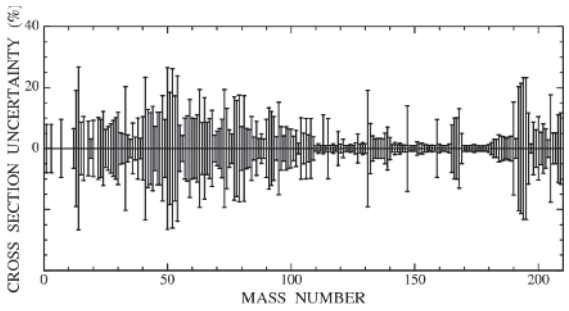

Figure 7. Presently quoted uncertainties for the stellar (n,γ) cross sections for $kT = 25$ keV (data from the KADoNiS compilation [54].

are clearly required, especially in the mass regions below $A = 120$ and above $A = 180$, where a large number of cross sections with uncertainties in excess of 10% await improvement. The situation sketched in Fig. 7 refers to thermal energies of $kT = 25 - 30$ keV, which are characteristic for He burning temperatures, but is generally worse for C shell burning in massive stars with $kT = 90$ keV.

Recent improvements for *s*-process related neutron capture measurements are based on the development of experimental techniques with optimized sensitivity and high granularity [8, 55]. Prominent examples mentioned before are 4π arrays for TOF measurements, large segmented HPGe detectors for γ counting, and the use of AMS techniques. In the field of laboratory neutron sources, significant progress has been achieved with respect to neutron flux and luminosity. High intensity, low-energy pulsed RFQ accelerators using the ^{7}Li$(p,n)^7$Be reaction for neutron production are under construction at Frankfurt [56] and Jerusalem [57], which will provide more than 100 times higher fluxes that previous Van de Graaff machines. In many complementary ways, high-energy spallation facilities have been demonstrated over the last decade to provide intense pulsed "white" neutron spectra. The latest success in this field is the construction of a new short flight path at CERN [58]. The development of high-flux facilities opens completely new opportunities for measurements on unstable branch point isotopes, where samples are extremely rare and sample activities have to be kept at a manageable level.

6 Summary

The slow time scale of the *s* process, which implies neutron capture times of typically a year, restrains the reaction flow within the valley of beta stability with the consequence that the resulting *s* abundances are determined by the neutron capture cross sections averaged over the thermal neutron spectra of the respective stellar scenarios. Therefore, laboratory measurements of neutron capture cross sections in the keV-energy range allows one to deduce the stellar Maxwellian average cross sections either via time-of-flight techniques or directly by activation in quasi-stellar neutron fields. Examples of such measurements including the opportunities offered by accelerator mass spectrometry were used to illustrate the direct impact of neutron capture studies on the *s*-process contribution to galactic chemical evolution as well as the unbiased information on the physical properties of the stellar *s*-process sites that can be derived from *s*-process branchings.

References

[1] E. Burbidge, G. Burbidge, W. Fowler, F. Hoyle, Rev. Mod. Phys. **29**, 547 (1957)
[2] A. Cameron, Tech. rep., A.E.C.L. Chalk River, Canada (1957)
[3] R. Gallino, C. Arlandini, M. Busso, M. Lugaro, C. Travaglio, O. Straniero, A. Chieffi, M. Limongi, Ap. J. **497**, 388 (1998)
[4] S. Merrill, Science **115**, 484 (1952)
[5] C. Raiteri, R. Gallino, M. Busso, D. Neuberger, F. Käppeler, Ap. J. **419**, 207 (1993)
[6] T. Rauscher, A. Heger, R. Hoffman, S. Woosley, Ap. J. **576**, 323 (2002)
[7] M. Arnould, S. Goriely, Phys. Rep. **384**, 1 (2003)
[8] F. Käppeler, R. Gallino, S. Bisterzo, W. Aoki, Rev. Mod. Phys. **83**, 157 (2011)
[9] M. Wiescher, F. Käppeler, K. Langanke, Ann. Rev. Astron. Astrophys. **50**, 165 (2012)
[10] T. Rauscher, F.K. Thielemann, Atomic Data Nucl. Data Tables **75**, 1 (2000)
[11] S. Goriely, *The role of nuclear models in providing nuclear data for astrophysics*, in *Long term needs for nuclear data development*, edited by M. Herman (IAEA, Vienna, 2001), pp. 83 – 94, report INDC(NDS)-428
[12] T. Rauscher, Ap. J. Lett. **755**, L10 (2012)
[13] K. Takahashi, K. Yokoi, Atomic Data Nucl. Data Tables **36**, 375 (1987)
[14] K. Yokoi, K. Takahashi, Nature **305**, 198 (1983)
[15] P. Lisowski, C. Bowman, G. Russell, S. Wender, Nucl. Sci. Eng. **106**, 208 (1990)
[16] U. Abbondanno, G. Aerts, H. Alvarez, S. Andriamonje, A. Angelopoulos, P. Assimakopoulos, C.O. Bacri, G. Badurek, P. Baumann, F. Becvar et al., Tech. rep., CERN, Geneva, Switzerland (2003), report CERN-SL-2002-053 ECT
[17] C. Guerrero, A. Tsinganis, E. Berthoumieux, *et al.*, Eur. Phys. J. A **49**, 27 (2013)
[18] http://j-parc.jp/, Tech. rep., JAERI and KEK (2004)
[19] K. Wisshak, F. Käppeler, Nucl. Sci. Eng. **77**, 58 (1981)
[20] Y. Nagai, M. Igashira, N. Mukai, T. Ohsaki, F. Uesawa, K. Takeda, T. Ando, H. Kitazawa, S. Kubono, T. Fukuda, Ap. J. **381**, 444 (1991)
[21] K. Wisshak, K. Guber, F. Käppeler, F. Voss, Nucl. Instr. Meth. A **299**, 60 (1990)
[22] M. Heil, R. Reifarth, M. Fowler, R. Haight, F. Käppeler, R. Rundberg, E. Seabury, J. Ullmann, J. Wilhelmy, K. Wisshak et al., Nucl. Instr. Meth. A **459**, 229 (2001)

[23] R. Reifarth, T.A. Bredeweg, A. Alpizar-Vicente, J.C. Browne, E.I. Esch, U. Greife, R.C. Haight, R. Hatarik, A. Kronenberg, J.M. O'Donnell et al., Nucl. Instr. Meth. A **531**, 530 (2004)

[24] K. Guber, R. Spencer, P. Koehler, R. Winters, Nucl. Phys. **A621**, 254c (1997)

[25] J. Klug, E. Altstadt, C. Beckert, R. Beyer, H. Freiesleben, V. Galindo, E. Grosse, A. Junghans, D. Legrady, B. Naumann et al., Nucl. Instr. Meth. A **577**, 641 (2007)

[26] R. Macklin, Nucl. Sci. Eng. **95**, 200 (1987)

[27] R. Plag, M. Heil, F. Käppeler, P. Pavlopoulos, R. Reifarth, K. Wisshak, Nucl. Instr. Meth. A **496**, 425 (2003)

[28] P. Koehler, R. Spencer, R. Winters, K. Guber, J. Harvey, N. Hill, M. Smith, Phys. Rev. C **54**, 1463 (1996)

[29] J. Tain, F. Gunsing, D. Cano-Ott, C. Domingo, J. Nucl. Sci. Tech. Suppl. **2**, 689 (2002)

[30] U. Abbondanno, G. Aerts, H. Alvarez, S. Andriamonje, A. Angelopoulos, P. Assimakopoulos, C.O. Bacri, G. Badurek, P. Baumann, F. Becvar et al., Nucl. Instr. Meth. Phys. Res. A **521**, 454 (2004)

[31] A. Borella, G. Aerts, G. F., A. Moens, R. Wynants, P. Schillebeeckx, *Determination of Weighting Functions and Neutron Sensitivity for C6D6 Detectors by MCNP*, in *Nuclear Data for Science and Technology*, edited by R. Haight, M. Chadwick, T. Kawano, P. Talou (AIP, New York, 2005), pp. 652–655, AIP Conference Series 769

[32] W. Ratynski, F. Käppeler, Phys. Rev. C **37**, 595 (1988)

[33] H. Beer, F. Käppeler, Phys. Rev. C **21**, 534 (1980)

[34] P. Mastinu, G. Martín Hernández, J. Praena, Nucl. Instr. Meth. A **601**, 333 (2009)

[35] G. Feinberg, M. Friedman, A. Krasa, A. Shor, Y. Eisen, D. Berkovits, G. Giorginis, T. Hirsh, M. Paul et al., Phys. Rev. C **85**, 055810 (2012)

[36] F. Käppeler, H. Beer, K. Wisshak, Rep. Prog. Phys. **52**, 945 (1989)

[37] P. Seeger, W. Fowler, D. Clayton, Ap. J. Suppl. **11**, 121 (1965)

[38] K. Wisshak, F. Voss, F. Käppeler, L. Kazakov, G. Reffo, Phys. Rev. C **57**, 391 (1998)

[39] C. Arlandini, F. Käppeler, K. Wisshak, R. Gallino, M. Lugaro, M. Busso, O. Straniero, Ap. J. **525**, 886 (1999)

[40] D. Lambert, V. Smith, M. Busso, R. Gallino, O. Straniero, Ap. J. **450**, 302 (1995)

[41] M. Busso, R. Gallino, G. Wasserburg, Ann. Rev. Astron. Astrophys. **37**, 239 (1999)

[42] S. Marrone, *et al.*, Phys. Rev. C **73**, 034604 (2006)

[43] K. Wisshak, F. Voss, F. Käppeler, M. Krtička, S. Raman, A. Mengoni, R. Gallino, Phys. Rev. C **73**, 015802 (2006)

[44] R. Reifarth, C. Arlandini, M. Heil, F. Käppeler, P. Sedyshev, M. Herman, T. Rauscher, R. Gallino, C. Travaglio, Ap. J. **582**, 1251 (2003)

[45] H. Nassar, M. Paul, I. Ahmad, D. Berkovits, M. Bettan, P. Collon, S. Dababneh, S. Ghelberg, J. Greene, A. Heger et al., Phys. Rev. Lett. **94**, 092504 (2005)

[46] G. Rugel, I. Dillmann, T. Faestermann, M. Heil, F. Käppeler, K. Knie, G. Korschinek, W. Kutschera, M. Poutivtsev, A. Wallner, Nucl. Inst. Meth. B **259**, 683 (2007)

[47] I. Dillmann, M. Heil, F. Käppeler, A. Wallner, W. Kutschera, A. Priller, P. Steier, M. Paul, Phys. Rev. C. **79**, 065805 (2009)

[48] I. Dillmann, T. Faestermann, G. Korschinek, J. Lachner, M. Maiti, M. Poutivtsev, G. Rugel, S. Walter, F. Käppeler, M. Erhard et al., Nucl. Instr. Meth. B **268**, 1283 (2010)

[49] A. Wallner, Nucl. Instr. Meth B **268**, 1277 (2010)

[50] H. Herndl, R. Hofinger, J. Jank, H. Oberhummer, J. Goerres, W. Wiescher, F.K. Thielemann, B. Brown, Phys. Rev. C **60**, 064614 (1999)

[51] T. Shima, F. Okazaki, T. Kikuchi, T. Kobayashi, T. Kii, T. Baba, N. Y., M. Igashira, Nucl. Phys. **A621**, 231c (1997)

[52] S. Raman, M. Igashira, Y. Dozono, S. H. Kitazawa, M. Mizumoto, J. Lynn, Phys. Rev. C **41**, 458 (1990)

[53] A. Wallner, K. Buczak, I. Dillmann, J. Feige, F. Käppeler, G. Korschinek, C. Lederer, A. Mengoni, U. Ott, M. Paul et al., Publications of the Astronomical Society of Australia **29**, 115 (2012)

[54] I. Dillmann, R. Plag, F. Käppeler, T. Rauscher, *KADoNiS v0.3 - The third update of the Karlsruhe Astrophysical Database of Nucleosynthesis in Stars*, in *EFNUDAT Fast Neutrons, Sci. Workshop on Neutron Measurements, Theory, and Applications*, edited by F.J. Hambsch (Publications Office of the European Union, Luxembourg, 2010), pp. 55 – 58, http://www.kadonis.org

[55] F. Käppeler, Prog. Part. Nucl. Phys. **66**, 390 (2011)

[56] O. Meusel, L. Chau, I. Mueller, U. Ratzinger, A. Schempp, K. Volk, C. Zhang, S. Minaev, *Development of an intense neutron source FRANZ in Frankfurt*, in *Linac 2006, Knoxville, USA* (http://accelconf.web.cern.ch/ AccelConf/106/PAPERS/MO051.PDF, 2006), p. 159

[57] A. Nagler, I. Mardor, D. Berkovits, K. Dunkel, M. Pekeler, C. Piel, P. vom Stein, H. Vogel, *Status of the SARAF Project*, in *2006 Linear Accelerator Conference*, (Joint Accelerator Conferences Website, JACoW, CERN, 2006), p. 168, http://www.JACoW.org/

[58] E. Chiaveri for the CERN n_TOF facility, *Neutron beam performances for cross section measurements*, in *Nuclear Data for Science and Technology* (2013)